Journal of Ceramic Processing Research. Vol. 26, No. 4, pp. 586~595 (2025)
(Received 8 May 2025, Received in revised form 12 June 2025, Accepted 3 July 2025)
https://doi.org/10.36410/jcpr.2025.26.4.586

J O U R N A L O F
Ceramic Processing Research

Green synthesis of CuO nanoparticles for photocatalytic applications: structural and optical characterization

Reyhan Gitmiş[a] and Ayça Tanrıverdi[a,b,*]
[a]*Department of Material Science and Engineering, Graduate School of Natural and Applied Sciences, Kahramanmaras Sutcu Imam University, Kahramanmaras, Türkiye*
[b]*Vocational School of Health Services, Dept. of Opticianry, Kahramanmaras Sutcu Imam University, Kahramanmaras, Türkiye*

Organic dye contamination in wastewater is a growing environmental threat that requires environmentally friendly and efficient treatment solutions. In this study, copper oxide nanoparticles (CuO NPs) were synthesized via an environmentally friendly method using *Ocimum basilicum* and *Solanum melongena* plant extracts. The resulting NPs exhibited different sizes (~50 nm and ~20 nm, respectively) and band gaps (2.26 eV and 1.94 eV), with characterization confirming their crystalline and nanoscale nature. Under solar light, *S. melongena* derived CuO NPs achieved superior photocatalytic degradation of methylene blue (92.27%) and brilliant blue (55.22%) dyes. These results highlight the promising role of plant-mediated CuO NPs as sustainable photocatalysts for wastewater remediation.

Keywords: Green synthesis, CuO NPs, Organic dye degradation, Photocatalysis, Kinetic mechanism.

Introduction

Population growth and industrial development have led to significant water pollution in recent years [1]. Various pollutants, including industrial waste, fertilizers, and pesticides, contaminate water sources [2]. Water treatment aims to make water suitable for specific uses by removing or reducing pollutants to acceptable levels [3]. The breakdown of organic pollutants through the use of light is acknowledged as a more favorable, economical, and eco-friendly approach in comparison to traditional advanced oxidation processes, such as ozone, hydrogen peroxide, and/or UV light treatment [4]. The development of effective photocatalytic materials has thus become a major research focus [1].

Nanotechnology plays a crucial role in this area by enabling the synthesis of advanced materials with tailored properties. Metal oxide nanoparticles (NPs), in particular, possess unique features such as tunable surface chemistry, morphology, and optical behavior, making them suitable for applications in health, environment, agriculture, and electronics [5–8]. However, conventional synthesis methods can be environmentally harmful, prompting the rise of green synthesis approaches [9].

Natural reducing and stabilizing agents, such as plant extracts, are used in green synthesis to produce NPs in a cost-effective and eco-friendly manner [10, 11]. Plant-based methods benefit from phytochemicals like flavonoids, phenols, terpenoids, and alkaloids, which influence the size, shape, and stability of NPs [12–16]. *Ocimum basilicum* (basil), from the Lamiaceae family, is rich in essential oils, flavonoids, phenolic compounds, and other bioactive molecules [17–22]. Recent studies conducted on *O. basilicum* have reported high total phenolic and flavonoid contents in aqueous extracts, with values of approximately 55.64 and 19.90 mg GAE/g, respectively, indicating its significant potential as a natural reducing and stabilizing agent in nanoparticle synthesis [23]. It is well established that these phytochemicals act as electron donors and metal chelators, facilitating the reduction of metal ions and preventing agglomeration during nanoparticle formation. Similarly, *Solanum melongena* (eggplant), a nutrient-rich vegetable from the Solanaceae family, contains anthocyanins, tannins, flavonoids, and copper making it a promising agent for the green synthesis of CuO NPs [24, 25]. In the study by Polat et al. (2024) [26], total phenolic content in different eggplant varieties ranged between 80.50 and 120.14 mg/kg. Additionally, GC-MS analysis identified 36 volatile aroma compounds in eggplant. The diverse phytochemicals in *O. basilicum* and *S. melongena* extracts act as natural reducing and stabilizing agents in the green synthesis of CuO NPs, enabling controlled particle formation and preventing aggregation. This sustainable approach supports the production of nanoparticles with effective photocatalytic properties for environmental applications. In this context, several recent studies have successfully demonstrated the

*Corresponding author:
Tel : +90 (344) 300-2815
Fax: +90 (344) 300 28 02
E-mail: aycatanriverdi@ksu.edu.tr

potential of green-synthesized CuO NPs in photocatalytic dye degradation systems. These works collectively highlight how plant-derived phytochemicals influence the structural, morphological, and photocatalytic properties of CuO NPs in environmental remediation applications. For instance, Aroob et al. [27] utilized a bio-mechanochemical approach with Seriphidium oliverianum leaf extract, yielding CuO NPs that achieved approximately 65% degradation of malachite green and methyl orange dyes under sunlight. Similarly, Jayasimha et al. [28] reported a green-synthesized CuO catalyst capable of degrading 97.35% of Acid Red 88 dye within 80 minutes of UV exposure, and additionally demonstrated its effective and application in ciprofloxacin sensing. In a comparative study, Gemachu and Birhanu [29] synthesized CuO, ZnO, and NiO NPs using Azadirachta indica extract, and found that CuO NPs exhibited the highest photocatalytic efficiency against methylene blue dye, underscoring their scalability and suitability for water treatment applications.

In this study, copper oxide (CuO) NPs were synthesized via a green route using aqueous extracts of *Ocimum basilicum* and *Solanum melongena* as natural reducing and stabilizing agents. The structural, morphological, and optical properties of the synthesized CuO NPs were characterized using X-ray diffraction (XRD), field emission scanning electron microscopy (FE-SEM), and Fourier-transform infrared spectroscopy (FT-IR), respectively. The photocatalytic performance of the CuO NPs was evaluated through the degradation of methylene blue (MB) and brilliant blue (BB) dyes under solar-simulated light using a 300 W xenon lamp. A comparative analysis was conducted to assess the impact of plant extract type on nanoparticle characteristics and photocatalytic efficiency. The results highlight the influence of phytochemical composition on both nanoparticle formation and their dye degradation capabilities, underscoring the potential of plant-mediated CuO NPs in sustainable water treatment applications.

Experimental

Copper(II) acetate monohydrate ($CuSO_4 \cdot 5H_2O$) was purchased from Merck, Methylene Blue (MB) ($C_{16}H_{18}ClN_3S$) vs. Brilliant Blue (BB) ($C_{37}H_{34}N_2Na_2O_9S_3$) was purchased from Sigma-Aldrich. *Ocimum basilicum* and *Solanum melongena* plants have been purchased from commercial sources. *Ocimum basilicum* and *Solanum melongena* plants were washed with tap water and then again with distilled water to remove dust and residue. After drying in the shade, the leaves, stems and stalks of the plants used in the experimental studies were ground to powder using a grinder. 10 g of plant powder was heated in 50 ml of distilled water at 50 °C for 60 min. The prepared solution was cooled to room temperature and then filtered with Whatman filter paper and the resulting stock extract was stored at 4 °C [25]. 50 ml of plant extract of *Ocimum basilicum* was heated to 70 °C with a magnetic stirrer. 2.41 g of copper (II) acetate monohydrate ($CuSO_4 \cdot 5H_2O$) was dissolved in 40 ml of pure water by stirring for 30 min in an ultrasonic bath. It was then added slowly to the plant extract. The solution was stirred overnight at 70 °C with a magnetic stirrer. The solution was centrifuged at 4000 rpm for 10 min to obtain the CuO NPs. It was left to dry at room temperature. The same procedure was followed for the plant extract of *Solanum melongena*. The synthesis steps of CuO NPs are shown in Fig. 1.

The morphology, shape, size and crystallographic structures of CuO NPs were investigated using a Zeiss Supra 55 FE-SEM (field emission scanning electron microscope). FT-IR analyses, which were used to investigate the molecular structure and interactions, were performed using PerkinElmer/MID Spectrum Two/ UATR. XRD measurements of CuO NPs were carried out using Rigaku, SmartLab. Photodegradation tests were carried out under 300W xenon lamp illumination using the solar simulator LuzChem-SolSim calibrated

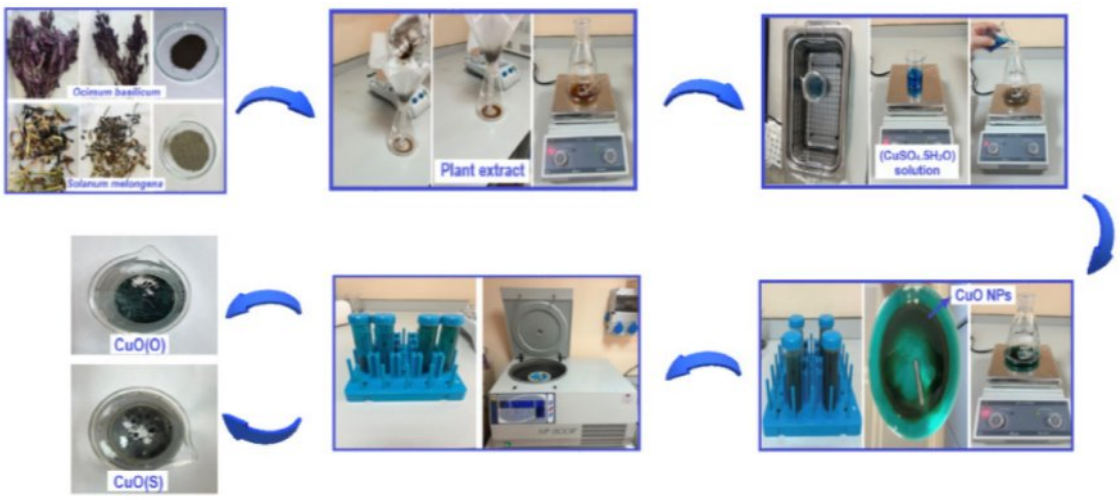

Fig. 1. CuO NP green synthesis steps.

AM1.5 spectra (ÜSKİM). Optical properties and photodegradation tests were investigated using UV-Vis spectrophotometer. UV-Vis analyses were investigated at KSÜ University-Industry-Public Cooperation Development Application and Research Center (ÜSKİM).

The photocatalytic activities of CuO(O) and CuO(S) NPs were determined by the degradation of MB and BB dyes using a solar simulator under 300 W visible light. For the photocatalytic degradation experiment, cationic dye solutions with a concentration of 20 ppm were prepared. 0.1 g of CuO NPs were added to the solutions obtained. The suspension was stirred in a sterile cabinet in the dark for 1 h to obtain the adsorption equilibrium of the contaminants before illumination. 2.5 ml of the suspension was taken with a pipette at 15 min intervals and analyzed using a UV-vis spectrophotometer.

The rate constant allows the determination of the photocatalytic activity, which is independent of the adsorption time and the concentration of the dye solution remaining in the solution. The Langmuir-Hinshelwood model can be applied to investigate the reaction kinetics of dye degradation. The L-H model is well established for heterogeneous photocatalysis at low dye concentration and is given in Eq. (1). The degradation efficiency of the dye solution can be calculated using Eq. (2) according to the Beer-Lambert law [30]:

$$In\left(\frac{C_t}{C_0}\right) = -k.t \quad (1)$$

$$Efficiency\ of\ degradation\ (\%) = \left(\frac{C_0 - C_t}{C_0}\right) \times 100 \quad (2)$$

In the equations, C_0 represents the initial concentration just before irradiation, C_t represents the concentration at the corresponding irradiation time, k represents the kinetic rate constant, and t represents the irradiation time [31]. The photocatalytic activities of CuO(R) and CuO(P) NPs were determined by investigating the degradation of MB and BB dyes as organic pollutants under visible light at 15 min intervals and at the end of 120 min. The degradation of dye solutions as a result of photocatalytic activity was kinetically studied, and the photocatalytic activity ratios were calculated.

Results and Discussion

The crystal structure of CuO(O) and CuO(S) NPs was investigated by X-ray diffraction pattern (Fig. 2). The diffraction peaks observed in both samples were in good agreement with the standard monoclinic CuO phase (JCPDS card no. 01-080-1268), confirming the successful synthesis of CuO NPs with monoclinic symmetry. Importantly, no additional peaks corresponding to secondary phases or impurities were detected, indicating the high phase purity of the synthesized CuO NPs [32].The hkl spatial orientations of the peaks observed at 32.53°, 35.47°, 38.72°, 48.93°, 53.48, 58.23°, 61.53°, 66.43°, 68.16°, 72.22° and 74.96° of 2θ

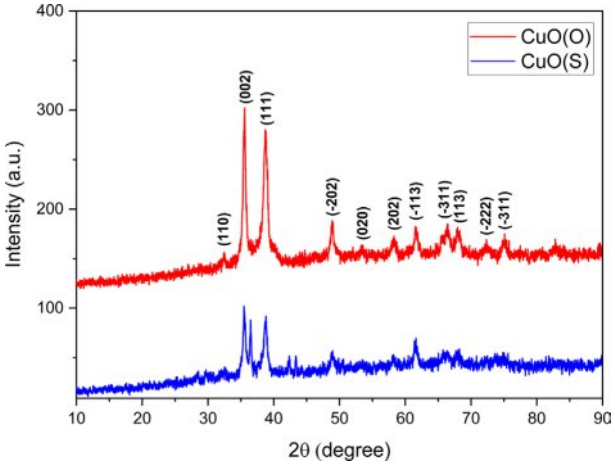

Fig. 2. XRD patterns of CuO(O) and CuO(S) NPs.

in the diffraction pattern of CuO(O) NPs correspond to the (110), (002), (111), ($\bar{2}$02), (020), (202), (1$\bar{1}$3), (31$\bar{1}$), (113) and ($\bar{2}$22) planes, respectively. The presence of the two sharpest peaks within the 2θ diffraction angles of 35.47° and 38.72° confirms the formation of monoclinic structured CuO NPs [33]. The spatial orientations of the peaks observed at 32.78°, 35.58°, 38.71°, 48.99°, 58.23°, 61.45°, 66.52° and 68.18° of 2θ for the CuO(S) diffraction pattern correspond to the (110), (002), (111), ($\bar{2}$02), (202), (1$\bar{1}$3), (31$\bar{1}$), and (113) planes, respectively. The XRD patterns of the same materials may be different. The peak positions may remain the same, but the peak intensities may be different. In particular, for nanoscale powder materials, the XRD peak intensities may decrease as the particle size decreases [34]. Using the Debye-Scherrer equation, the average crystal grain sizes of CuO(O) and CuO(S) NPs were calculated to be 13.86 nm and 7.62 nm, respectively.

The structural properties of CuO, NPs were analyzed by XRD, and the grain size of the nanoparticles was calculated by the Debye-Scherrer formula Eq. (3) using the graph obtained from the XRD pattern. According to the Debye-Scherrer formula, there is a relationship between the grain size and the width of the half-intensity [35].

$$D = \frac{k\lambda}{\beta cos\theta} \quad (3)$$

Where D is the grain size, λ (1.5418 A°) is the wavelength of CuKα radiation, β is the full width at half maximum (FWHM) and θ is the angle of Bragg diffraction [36]. Table 1 shows the XRD structural parameters of CuO NPs.

The morphology, structure, and dimensions of CuO(O) and CuO(S) NPs were investigated by FESEM images. The images were taken at magnifications of 100 nm. FE-SEM images clearly show that the morphology of CuO is composed of spherical clustered nanoparticles.

Table 1. XRD structural parameters of CuO NPs.

NPs	Observed values		Standard values		(hkl)	PDF card number	Faz
	2θ (°)	*d* (Å)	2θ (°)	*d* (Å)			
CuO(O)	32.53	2.75	32.53	2.74	(110)	01-080-1268	monoclinic (CuO)
	35.47	2.52	35.55	2.52	(002)	01-080-1268	monoclinic (CuO)
	38.72	2.32	38.96	2.30	(111)	01-080-1268	monoclinic (CuO)
	48.93	1.85	48.75	1.85	($\bar{2}$02)	01-080-1268	monoclinic (CuO)
	53.48	1.70	53.50	1.70	(020)	01-080-1268	monoclinic (CuO)
	58.23	1.58	58.35	1.57	(202)	01-080-1268	monoclinic (CuO)
	61.53	1.50	61.57	1.50	(11$\bar{3}$)	01-080-1268	monoclinic (CuO)
	66.43	1.40	65.84	1.42	(31$\bar{1}$)	01-080-1268	monoclinic (CuO)
	68.16	1.37	68.14	1.37	(113)	01-080-1268	monoclinic (CuO)
	72.22	1.30	72.42	1.30	($\bar{2}$22)	01-080-1268	monoclinic (CuO)
	74.96	1.26	75.82	1.26	(311)	01-080-1268	monoclinic (CuO)
CuO(S)	32.78	2.75	32.53	2.74	(110)	01-080-1268	monoclinic (CuO)
	35.58	2.52	35.55	2.52	(002)	01-080-1268	monoclinic (CuO)
	38.71	2.32	38.96	2.30	(111)	01-080-1268	monoclinic (CuO)
	48.99	1.86	48.75	1.85	($\bar{2}$02)	01-080-1268	monoclinic (CuO)
	58.23	1.58	58.35	1.57	(202)	01-080-1268	monoclinic (CuO)
	61.45	1.51	61.57	1.50	(11$\bar{3}$)	01-080-1268	monoclinic (CuO)
	66.52	1.40	65.84	1.42	(31$\bar{1}$)	01-080-1268	monoclinic (CuO)
	68.16	1.37	68.14	1.37	(113)	01-080-1268	monoclinic (CuO)

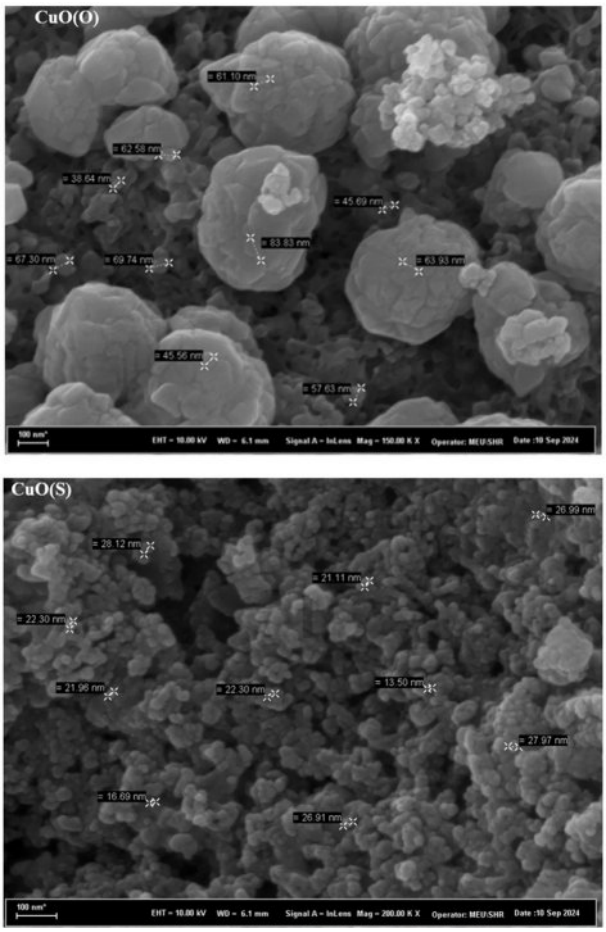

Fig. 3. FE-SEM images of CuO(O) and CuO(S) NPs.

The morphology of CuO NPs depends on plant-based stabilizers and reducing agents in green synthesis. The nucleation rate depends on supersaturation and active nucleation [37]. FE-SEM images of the CuO(O) and CuO(S) NPs are shown in Fig. 3. FE-SEM images showed that CuO(O) NPs were in a homogeneously distributed spherical structure, with a size of about 50 nm. FE-SEM images showed that CuO(S) NPs were in a homogeneously distributed spherical structure with a size of approximately 20 nm. The anthocyanins, phenolic compounds, and saponins found in the *Solanum melongena* plant may have caused the formation of the smaller size CuO(P) NPs. This is because these compounds may have accelerated nucleation during synthesis, while causing the particles to become smaller. In addition, nano-sized materials have a more active surface area than micron-sized CuO. In this case, they provide a more efficient photocatalytic effect because more light absorption occurs**.**

The FT-IR spectra of the CuO(O) and CuO(S) NPs are shown in Fig. 4. The IR bands at 414 and 484 cm^{-1} determine the stretching vibrations of the Cu-O bond in monoclinic CuO. The presence of a distinct IR band around 400-600 cm^{-1} confirms the formation of CuO from the green synthesis [38]. The peaks between 900-1100 cm^{-1} represent the asymmetric and unsymmetric stretching of the C-O-C bond. The peaks at 944 and 1014 cm^{-1} may indicate the presence of C-O-C stretching vibrations in flavonoids, polysaccharides and other organic compounds from plant extracts. The peaks around 2200-

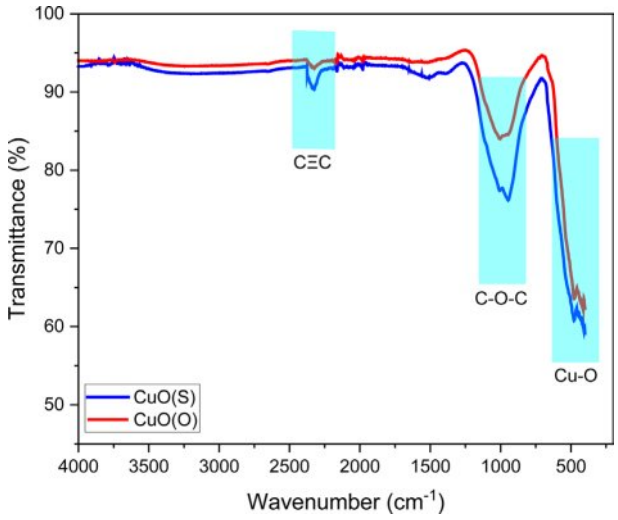

Fig. 4. FT-IR spectra of CuO(O) and CuO(S) NPs.

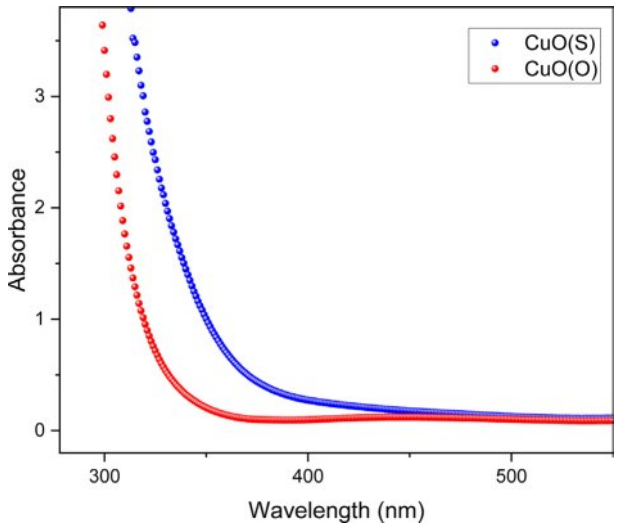

Fig. 5. UV absorbance spectra of CuO(O) and CuO(S) NPs.

2400 cm^{-1} may represent the CΞC (alkyne) stretching vibrations, which are long-chain carbon compounds in the sample originating from plant organic residues. It usually appears as a weak signal.

The optical properties of CuO(O) and CuO(S) NPs were investigated by means of absorption spectra using UV-Vis spectrophotometer. Fig. 5 shows the optical absorption spectra of CuO(O) and CuO(S) NPs. The optical absorption spectra were measured in the range of 200 to 800 nm. The absorption band which is maximum at 300-350 nm indicates the presence of CuO nanostructure [39]. The optical absorption, which is caused by the excitation of electrons from the valence band to the conduction band of CuO, causes a decrease in the wavelength. It was observed that the optical absorption decreases smoothly from UV to near.

The energy band gap (Eg) of CuO NPs was calculated using Tauc's formula Eq. (4) [40].

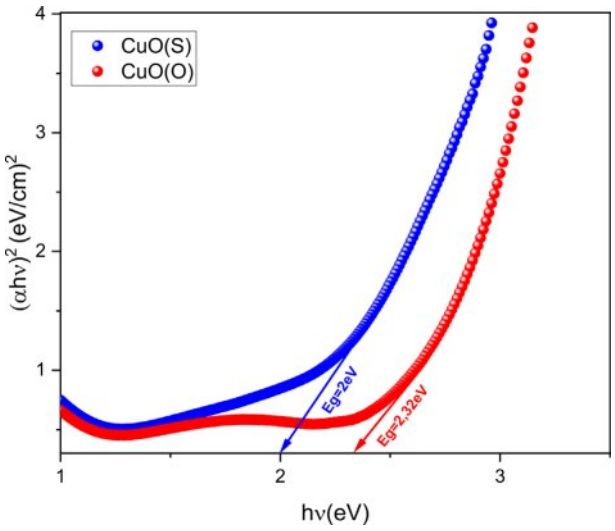

Fig. 6. Tauc curves of CuO(O) and Cuo(S) NPs.

$$(\alpha h\nu)_2 = A(h\nu - Eg) \quad (4)$$

In the formula, αhν is the absorption coefficient, hν is the energy of the photon, and A is the value of the energy constant [41]. Tauc plots for CuO(O) and CuO(S) NPs are shown in Fig. 6. The Eg values were estimated from the intersection of the linear portion. Eg values of CuO(O) and CuO(S) NPs were calculated to be 2.26 eV and 1.94 eV, respectively.

Photocatalytic degradations of CuO NPs, prepared by green synthesis, by synthetic organic pollutants MB and BB was investigated by using a solar simulator under 300 W xenon visible light at room temperature. The degradation of CuO NPs in cationic dyes was studied by taking measurements every 15 min. The photodegradation tests were performed using a scanning UV-Vis spectrophotometer in the range of 400-800 nm.

The variation of the UV absorption spectra of the synthesized CuO(O) NPs for photocatalytic degradation of MB with respect to time is shown in Fig. 7a. A consistent decrease in absorbance with increasing irradiation time indicates a reduction in MB concentration. The degradation efficiencies at 15, 30, 45, 60, 75, 90, 105, and 120 minutes were calculated as 28.54%, 43.42%, 51.36%, 56.51%, 61.04%, 63.96%, 68.92%, and 82.69%, respectively. A rapid initial degradation was observed within the first 30 minutes, likely due to the abundance of active surface sites and rapid generation of reactive oxygen species (ROS). The degradation rate slowed between 45 and 90 minutes, potentially due to site saturation and reduced dye concentration. An acceleration in the final phase suggests enhanced degradation of intermediates and smaller by-products. These results confirm the photocatalytic activity of CuO(O) NPs.

A progressive decline in the degree of absorption with an increase in the duration of the irradiation is

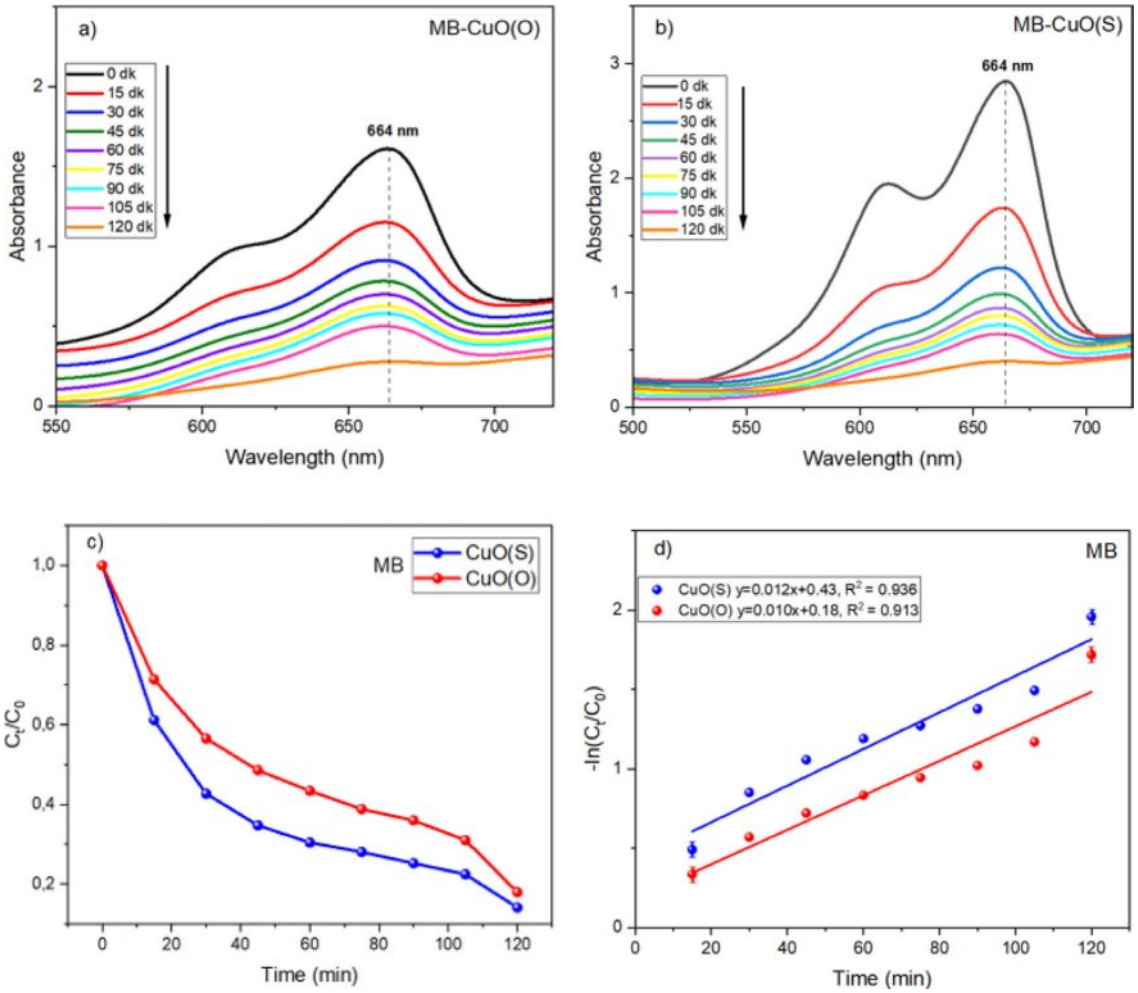

Fig. 7. (a) CuO(O) and (b) CuO(S) degradation of MB dye under UV-vis irradiation, (c) CuO(O) and CuO(S) NP catalysts degradation efficiencies, (d) rate constants of CuO(O) and CuO(S) NP.

indicative of a reduction in the concentration of MB. [42] The degradation efficiencies at 15, 30, 45, 60, 75, 90, 105, and 120 minutes were determined as 38.86%, 57.27%, 65.25%, 69.57%, 71.96%, 74.77%, 77.72%, and 92.27%, respectively. A notable 38.86% degradation occurred within the first 15 minutes, indicating rapid initial interaction between CuO(S) NPs and MB. The slower degradation observed between 30 and 105 minutes may be attributed to decreased MB concentration and the saturation of active catalytic sites. In the final 15 minutes, the degradation rate increased markedly, suggesting renewed photocatalytic activity, likely due to the breakdown of intermediates and further oxidation of residual dye molecules. These findings confirm the effective photocatalytic performance of green-synthesized CuO(S) NPs.

When exposed to sunlight in the presence of CuO nanocatalysts (NCs), the strong MB band at 664 nm starts to decrease and the strong peak starts to decrease. The photodegradation activities of the cationic dyes of MB in the presence of CuO(O) and CuO(S) catalysts are shown in Fig. 7c. During the photodegradation experiment, it was found that the color of MB gradually changed from blue to colorless with the increase of irradiation time, and the degradation effect was consistent with the removal rate result of MB [43]. The degradation efficiency of CuO(O) catalyst reached 82% after 120 min. Meanwhile, the degradation efficiency of CuO(S) catalyst reached 92% after 120 min of irradiation. It can be clearly seen that CuO(S) NC showed higher photocatalytic performance. The results also showed that CuO(O) NC was also effective, but not as efficient as CuO(S). This may be due to the smaller particle size of CuO(S) catalyst (20 nm), which increases the surface area and improves the photocatalytic efficiency. In addition, CuO(S) NPs have a lower bandgap energy value (Eg=1.94 eV), which indicates a wider light absorption range. Therefore, they can absorb photons with longer wavelengths and can absorb more photons in the visible light region. This results in a more effective photocatalytic activity under sunlight. When CuO(S) absorbs photons, electrons in the valence band can more easily pass into the conduction band. This allows for the production of more e--h^+ pairs, resulting in higher production of reactive species

(OH·, O_2^-, etc.). These reactive species, particularly hydroxyl radicals (·OH) and superoxide anions (O_2^-·), play a critical role in the degradation mechanism. Upon sunlight irradiation, CuO NPs generate electron-hole pairs (e^-/h^+), where the excited electrons reduce molecular oxygen to O_2^-·, while the holes oxidize water or hydroxide ions to form ·OH. These highly reactive species subsequently attack the dye molecules, breaking the chromophoric structures via oxidative cleavage, leading to mineralization into less harmful end-products such as CO_2 and H_2O. This mechanism explains the gradual decolorization and reduction in absorbance of the dye solutions observed in the UV-Vis spectra [44, 45]. In Fig. 7d, the photodegradation kinetics of MB degradation of CuO(O) and CuO(S) NCs were determined by plotting the -In(C_t/C_0) curve against the reaction time (time) to determine the pseudo first order reaction kinetics. The ratio of -ln(C_t/C_0) is directly proportional to the contact time. This ratio also shows that photocatalytic degradation of MB solution is directly proportional to MB dye concentration [46]. It can be seen from the graph that k = 0.010 min^{-1} for CuO(O) and k = 0.012 min^{-1} for CuO(S). The reaction rate constant (k) for CuO(S) is larger than CuO(O). Faster photocatalytic degradation is indicated by a higher k value. Since CuO(S) has smaller band gap (Eg), a photocatalyst with broader spectrum of light absorption and a longer lifetime of the charge carriers can be explained by the faster degradation of MB. How well the model fits the data is indicated by the R^2 (coefficient of determination). Fig. 7d shows R^2 = 0.913 for CuO(O) and R^2 = 0.936 for CuO(S). Although both of these models show a good fit, the CuO(S) model provides a more reliable model because its R^2 value is higher. As the R^2 value gets closer to 1, fit between the linear regression model and the experimental data increases.

In Fig. 8d, the photodegradation kinetics of CuO(O) and CuO(S) NCs for BB degradation were determined by plotting the -In(Ct/C0) curve against the reaction time (time) to determine the pseudo-first order reaction kinetics. From the graph, it can be observed that k = 0.003 min^{-1} for CuO(O) and k = 0.007 min^{-1} for CuO(S). These values indicate that CuO(S) provides about more than 2 times faster degradation as compared to CuO(O).

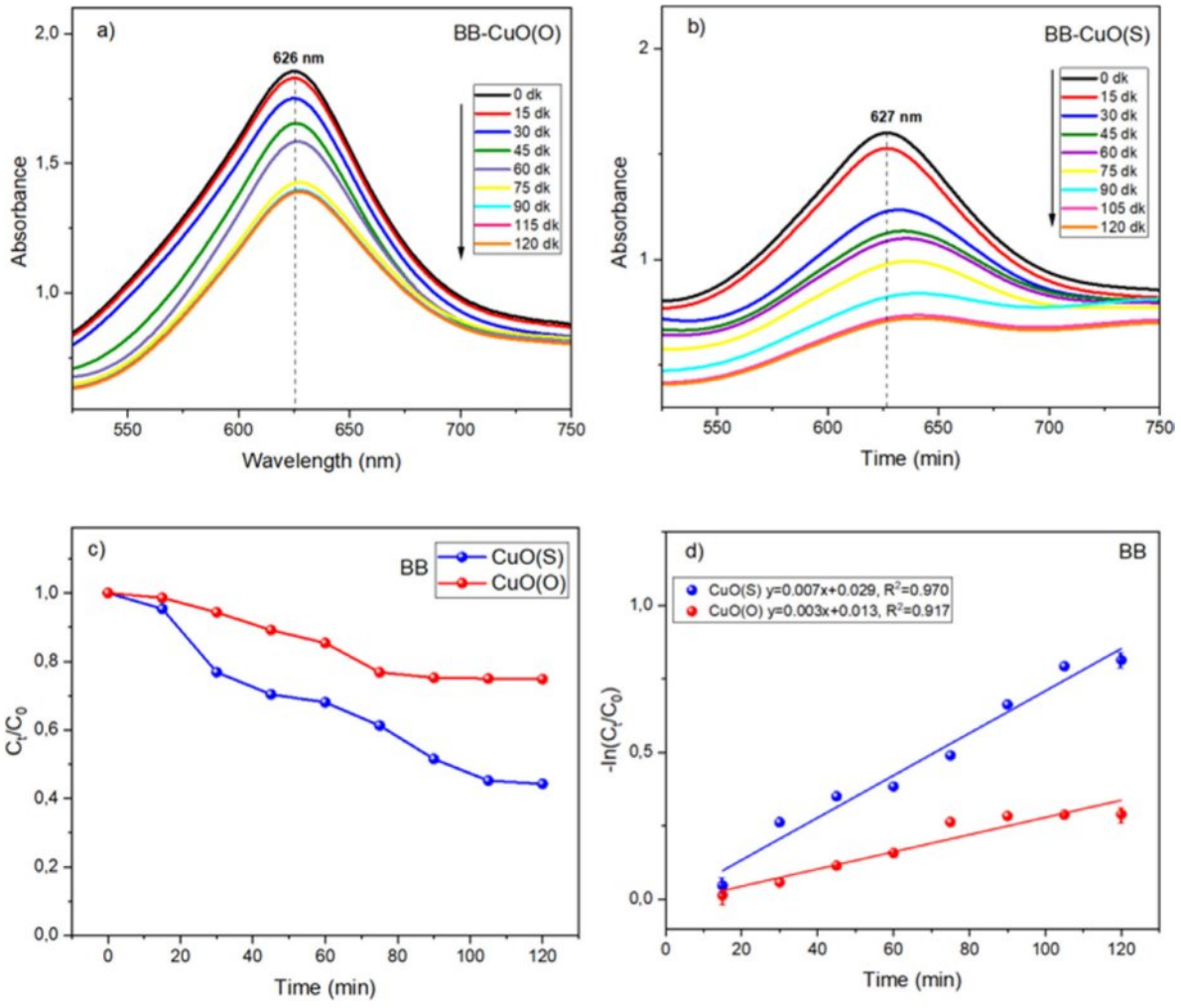

Fig. 8. (a) CuO(O) and (b) CuO(S) degradation of BB dye under UV-vis irradiation, (c) CuO(O) and CuO(S) NP catalysts degradation efficiencies, (d) rate constants of CuO(O) and CuO(S) NP.

Table 2. Comparative study of photocatalytic degradation of dyes using CuO based materials.

Plant Extract	Photo catalyst	Dye	Time (min)	Degradation Efficiency (%)	Ref.
1. *Aloe barbadensis miller*	CuO	MB	60	92	[52]
		RhB	60	76	
2. *Papaya peel*	CuO NP	MB	90	27	[53]
Banana peel		MB	90	26	
3. *Seriphidium oliverianum*	CuO NP	MG	60	65	[27]
		MO	60	65	
4. *Citrus limon*	CuO NP	MB	80	87	[54]
5. *Papaya bark*	PB-CuO NP	RhB	120	93	[55]
Banana stem		EY	120	94	
	BS-CuO NP	RhB	120	94	
		EY	120	96	
6. *Ocimum basilicum*	CuO(O) NP	MB	120	82	This work
Solanum melongena		BB	120	25	
	CuO(S) NP	MB	120	92	
		BB	120	56	

Therefore, CuO(S) can be considered as a more efficient photocatalyst for the degradation of BB dye. Fig. 8d shows that the R^2 value for CuO(O) is 0.917 and the R^2 value for CuO(S) is 0.970. The R^2 value of 0.970 indicates that the degradation process by CuO(S) fits the first-order kinetic model fairly well.

Figure 8 shows the time-dependent UV absorption spectra for the photocatalytic degradation of BB dye using (a) CuO(O) and (b) CuO(S) NCs. Initially, BB exhibits maximum adsorption in the dark, followed by gradual degradation under sunlight, indicating a reduction in dye concentration. For CuO(O) (Fig. 8a), degradation increased slowly, reaching only 25.27% after 120 minutes, with the system approaching equilibrium in the final 30 minutes suggesting limited photocatalytic efficiency. In contrast, CuO(S) (Fig. 8b) showed a more rapid increase, particularly after 30 minutes, reaching 55.90% degradation at 120 minutes. The initial lag phase reflects the activation time of the catalyst surface, while the plateau after 105 minutes suggests saturation of the photocatalytic process. Overall, CuO(S) exhibited higher efficiency than CuO(O), though its activity toward BB remained moderate. Fig. 8c compares the BB dye degradation efficiencies of CuO(O) and CuO(S) catalysts. CuO(O) showed limited activity, reaching only 25% after 120 minutes, likely due to weak interaction with the dye. In contrast, CuO(S) achieved 55% degradation, with a notable 23.29% in the first 30 minutes, indicating higher initial and overall photocatalytic efficiency. Table 2 provides a comparative overview of CuO-based photocatalysts synthesized by green methods using various plant extracts evaluated under sunlight. This eco-friendly approach is in line with sustainable chemistry and demonstrates efficient dye degradation against pollutants such as MB, BB, RhB (Rhodamine B), EY (Eosin yellow), MG (methylene green) and MO (methylene orange). While degradation efficiencies vary based on the plant source and dye type, the CuO(S) NPs synthesized using *Solanum melongena* in this study exhibited high photocatalytic activity, degrading 92% of MB and 56% of BB within 120 min. These results are similar or better than many previously reported green synthesized CuO materials and confirm the potential of plant-mediated synthesis under solar conditions for effective photocatalytic applications. To put the photocatalytic performance of the synthesized CuO(S) and CuO(O) NPs into context, Table 2 presents a comparison of green-synthesized CuO-based photocatalysts reported in the literature, prepared using various plant extracts and evaluated under sunlight irradiation. This eco-friendly strategy aligns with the principles of sustainable chemistry and has been shown to effectively degrade a range of organic dyes, including Methylene Blue (MB), Brilliant Blue (BB), Rhodamine B (RhB), Eosin Yellow (EY), Methylene Green (MG), and Methyl Orange (MO). In this study, CuO(S) NPs synthesized from *Solanum melongena* exhibited significant photocatalytic activity, achieving notable degradation efficiencies of 92% for MB and 56% for BB within 120 minutes. These results are comparable or superior to many reported CuO-based systems, highlighting plant-mediated synthesis under solar irradiation as a sustainable and promising route for high-performance photocatalytic applications.

The proposed photodegradation mechanism of MB and BB dyes using CuO NCs is illustrated in Fig. 9. Upon light irradiation with energy greater than the CuO band gap, electrons (e^-) are excited from the valence band (VB) to the conduction band (CB), generating

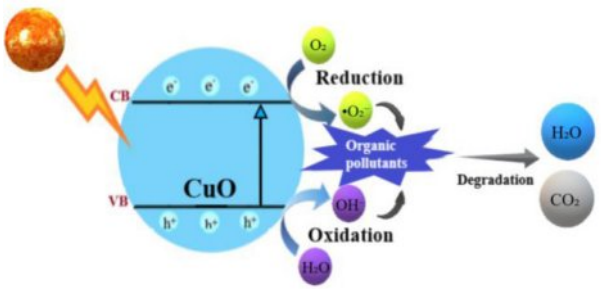

Fig. 9. Schematic representation of the dye degradation mechanism.

electron-hole pairs (eq. 5) [47]. The excited electrons react with molecular oxygen to form superoxide radicals ($\bullet O_2^-$) (eq. 6) [48], while the holes oxidize water or hydroxide ions to generate hydroxyl radicals (•OH) (eq. 7–8) [49]. These reactive oxygen species (•OH and $\bullet O_2^-$) play a key role in degrading organic pollutants into non-toxic end products like CO_2 and H_2O (eq. 9) [50, 51].

$$CuO\ NP + h\nu \rightarrow e^- + h^+ \quad (5)$$

$$e^- + O_2 \rightarrow \bullet O_2^- \quad (6)$$

$$h^+ + H_2O \rightarrow \bullet OH + H^+ \quad (7)$$

or

$$h^+ + OH^- \rightarrow \bullet OH \quad (8)$$

$$\bullet OH + (MB \text{ or } BB) \rightarrow CO_2 + H_2O \text{ or } \bullet O_2^- + (MB \text{ or } BB) \rightarrow CO_2 + H_2O \quad (9)$$

Conclusion

This study demonstrated the successful green synthesis of CuO NPs using *Ocimum basilicum* and *Solanum melongena* extracts, revealing significant differences in particle size, band gap energy, and photocatalytic activity. Among the two, CuO(S) NPs exhibited superior photocatalytic degradation, particularly for methylene blue, achieving up to 92.27% efficiency. The enhanced activity is likely due to the rich phytochemical profile of *S. melongena*, which facilitates the formation of smaller, more reactive nanoparticles. While similar studies exist, this work is distinctive in its comparative approach using two different plant species for CuO synthesis under identical conditions. The findings underline the potential of plant-based CuO NPs especially those derived from *S. melongena* as effective, low-cost, and sustainable photocatalysts for water treatment. This study contributes valuable insight into the influence of biological source on photocatalytic performance, supporting further exploration of plant diversity in nanomaterial synthesis.

Acknowledgment

This study was prepared by Reyhan GİTMİŞ from her master's thesis entitled 'Production of copper oxide nanoparticles by green synthesis and investigation of their photocatalytic performance' prepared at Kahramanmaraş Sütçü İmam University, Institute of Science. Thesis Supervisor: Asst. Prof. Ayça TANRIVERDİ

Corresponding Author

Ayça Tanrıverdi (https://orcid.org/0000-0002-0658-8576) aycatanriverdi@ksu.edu.tr

Funding

This study was not funded by any supporter

Conflict of interest

All authors certify that they have no affiliations with or involvement in any organization or entity with any financial interest or non-financial interest in the subject matter or materials discussed in this manuscript.

Author contributions

Conceptualization: Ayça Tanriverdi; Methodology: Ayça TANRIVERDİ, Reyhan GİTMİŞ; Formal analysis and investigation: Ayça TANRIVERDİ, Reyhan GİTMİŞ; Writing - original draft preparation: Ayça TANRIVERDİ, Reyhan GİTMİŞ; Writing - review and editing: Ayça TANRIVERDİ, Reyhan GİTMİŞ

References

1. M.A. Al-Nuaim, A.A. Alwasiti, and Z.Y. Shnain, Chem. Pap. 77[2] (2023) 677-701.
2. D. Akhil, D. Lakshmi, A. Kartik, D.V.N. Vo, J. Arun, and K.P. Gopinath, Environ. Chem. Lett. 19 (2021) 2261-2297.
3. S.G. Akpe, I. Ahmed, P. Puthiaraj, K. Yu, and W.S. Ahn, Micropor. Mesopor. Mat. 296 (2020) 109979.
4. M. Ji and Y.I. Lee, J. Ceram. Process. Res. 22[4] (2021) 386-393.
5. I. Ali, A. Kucherova, N. Memetov, T. Pasko, K. Ovchinnikov, V. Pershin, D. Kuznetsov, E. Galunin, V. Grachev, and A. Tkachev, J. Mol. Liq. 279 (2019) 251-266.
6. S.J. Anwar, H.M. Yusoff, I.U.H. Bhat, and L.K. Ern, Arab. J. Sci. Eng. 49[1] (2024) 475-496.
7. G. Gürsoy, Z. Çiçek, S. Tekerek, E. Kiray, A. Tanriverdi, and E. Çakmak, Appl. Organomet. Chem. 38[6] (2024) e7492.
8. V. Ramya, V. Kalaiselvi, S.K. Kannan, M. Shkir, H.A. Ghramh, Z. Ahmad, N. Vidhya, P. Nithiya, Arab. J. Sci. Eng. 47[1] (2022) 909-918.
9. L. Soltys, O. Olkhovyy, T. Tatarchuk, and M. Naushad, Magnetochemistry 7[11] (2021) 145.
10. S. Vijayaram, H. Razafindralambo, Y.Z. Sun, S. Vasantharaj, H. Ghafarifarsani, S.H. Hoseinifar, and M. Raeeszadeh, Biol. Trace Elem. Res. 202[1] (2024) 360-386.
11. I. Sugihartono, R.O.A. Azzahra, N. Yudasari, E. Budi, R. Fahdiran, W. Indrasari, and A. S. Budi, J. Ceram. Process. Res. 25[4] (2024) 557-562.
12. G. Benelli, Parasitol. Res. 114[9] (2015) 3201-3212.
13. A.M.E. Shafey, Green Process. Synth. 9[1] (2020) 304-339.
14. Z. Aguilar, Nanomaterials for Medical Applications, Newnes, New York (2012).
15. V. Soni, P. Raizada, P. Singh, H.N. Cuong, A. Saini, R.V. Saini, and V.H. Nguyen, Environ. Res. 202 (2021) 111622.
16. J.O. Adeyemi, A.O. Oriola, D.C. Onwudiwe, and A.O.

Oyedeji, Biomolecules 12[5] (2022) 627.
17. A. Omidtorshiz, M.R. Benam, M. Momennezhad, Z. Sabouri, and M. Darroudi, Inorg. Chem. Commun. 158 (2023) 111575.
18. N.S. Azizah, B. Irawan, J. Kusmoro, W. Safriansyah, K. Farabi, D.F. Oktavia, and M. Miranti, Plants 12[24] (2023) 4148.
19. R.H. Saadabadi, F.S. Tehrani, Z. Sabouri, and M. Darroudi, Inorg. Chem. Commun. 168 (2024) 112955.
20. S.U.R. Qamar, K. Virijević, D. Arsenijević, E. Avdović, M. Živanović, N. Filipović, A. Ćirić, and I. Petrović, Colloid Interfac. Sci. 59 (2024) 100771.
21. R.H. Saadabadi, F.S. Tehrani, Z. Sabouri, and M. Darroudi, Sci. Rep-UK 14 (2024) 29812.
22. M. Nasrollahzadeh, F. Ghorbannezhad, and S.M. Sajadi, Appl. Organomet. Chem. 33[1] (2019) e4698.
23. H. Kanmaz, Y. Gokce, and A.A. Hayaloglu, Food Chem. Adv. 3 (2023) 100429.
24. J. Komara, J.P. Karumuri, and B.S.S. Naik, Hybrid Adv. 7 (2024) 100304.
25. A. Solmaz, T. Turna, and A. Baran, Biomass Convers. Bior. 14[9] (2024) 10771-10789.
26. H.E. Polat, O. Zambi, Y. Güçer, and A.S. Anli, Ital. J. Food Sci. 36[3] (2024) 1-10.
27. S. Aroob, S.A. Carabineiro, M.B. Taj, I. Bibi, A. Raheel, T. Javed, and M. Sillanpää, Catalysts 13[3] (2023) 502.
28. H.N. Jayasimha, K.G. Chandrappa, P.F. Sanaulla, and V.G. Dileepkumar, Sensors Int. 5 (2024) 100254.
29. L.Y. Gemachu and A.L. Birhanu, Green Chem. Lett. Rev. 17[1] (2024) 2293841.
30. D. Zhang, F. Dai, P. Zhang, Z. An, Y. Zhao, and L. Chen, Mater. Sci. Eng. C 96 (2019) 684-692.
31. Y.S. Song, D.Y. Lee, B. Kim, and D.Y. Lee, J. Ceram. Process. Res. 20[2] (2019) 182-186.
32. L. Kunhikrishnan, and R. Shanmugam, J. Mater. Sci: Mater. Electron. 31[23] (2020) 21528-21539.
33. T. Saha, M.B. Mobarak, M.N. Uddin, M.S. Quddus, M.R. Naim, and N.S. Pinky, Mater. Chem. Phys. 305 (2023) 127979.
34. C.F. Holder and R.E. Schaak, ACS Nano 13[7] (2019) 7359-7365.
35. B.D. Cullity and S.R. Stock, Elements of X-ray Diffraction, Prentice Hall, New York (2001).
36. F. Saadaoui, S. Sayouri, A. Rjeb, B. Akharkhach, and A. Nfissi, J. Ceram. Process. Res. 20[2] (2019) 139-142.
37. S. Karthika, P. Kanchana, B.P. Devi, and S.S. Sundari, Inorg. Nano. Met. Chem. 54[5] (2024) 458-466.
38. S. Tekerek, F. Göde, and E.B. Yılmaz, J. Ceram. Process. Res. 26[2] (2025) 286-294.
39. G. Manjari, S. Saran, T. Arun, A.V.B. Rao, and S.P. Devipriya, J. Saudi Chem. Soc. 21[5] (2017) 610-618.
40. J. Tauc (Ed.), Amorphous and Liquid Semiconductors, Springer, New York (2012).
41. J. Klein, L. Kampermann, B. Mockenhaupt, M. Behrens, J. Strunk, and G. Bacher, Adv. Funct. Mater. 33[47] (2023) 2304523.
42. H.H. Nguyen, G. Gyawali, and B. Joshi, J. Ceram. Process. Res. 23[1] (2022) 33-40.
43. V. Natarajan, K. Sathiyamoorthy, R. Thilak Kumar, M. Navaneethan, and S. Harish, J. Mater. Sci: Mater. Electron. 35[1] (2024) 25.
44. A.K. Sibhatu, G.K. Weldegebrieal, S. Sagadevan, N.N. Tran, and V. Hessel, Chemosphere 300 (2022) 134623.
45. J.C. de Almeida, T.A. Rodrigues, G.T. da Silva, C. Ribeiro, and V.R. de Mendonça, Mater. Adv. 5[16] (2024) 6479-6488.
46. K A. Isai and V.S. Shrivastava, SN Appl. Sci. 1 (2019) 1-11.
47. P.S. Nandisha, Mater. Sci. Eng. B 295 (2023) 116607.
48. H. Bibi, M. Iqbal, H. Wahab, M. Öztürk, F. Ke, Z. Iqbal, M.I. Khan, ad S.M. Alghanem, Sci. Rep-UK 11[1] (2021) 10781.
49. A. Atri, M. Echabaane, A. Bouzidi, I. Harabi, B.M. Soucase, and R.B. Chaâbane, Heliyon 9[2] (2023) e13484.
50. T. Liu, L. Wang, X. Lu, J. Fan, X. Cai, B. Gao, and Y. Lv, RSC Adv. 7[20] (2017) 12292-12300.
51. K. Sahu, J. Singh, and S. Mohapatra, Opt. Mater. 93 (2019) 58-69.
52. B. Uma, K. S. Anantharaju, L. Renuka, S. Malini, S.S. More, Y.S. Vidya, and S. Meena, Ceram. Int. 47[7] (2021) 10355-10369.
53. P. Koteeswari, S. Sagadevan, I. Fatimah, A.K. Sibhatu, S.I. Abd Razak, E. Leonard, and T. Soga, Inorg. Chem. Commun. 144 (2022) 109851.
54. S. Reshma, H. Shaik, K. Venkatesan, M.D. Kadeer, and P.V. Somaiah, Russ. J. Gen. Chem. 94[1] (2024) 220-233.
55. S. Borgayary, N. Das, R.R. Wary, M.B. Baruah, S. Basumatary, B. Das, and P. Kalita, Inorg. Chem. Commun. (2025) 114664.